Asian Journal of Chemistry; Vol. 35, No. 8 (2023), 1836-1842

ASIAN JOURNAL OF CHEMISTRY

https://doi.org/10.14233/ajchem.2023.28026

Hydrothermal Synthesis and Micro-Structural, Optical and Luminescence Properties of Core-Shell Hetero Structure CdS/$Zn_3(PO_4)_2$ Nanocomposite

G. Sreedevi[1], T. Pullarao[1], S.K. Khaja Muswareen[2], S. Suresh[3], P. Vijaya Sirisha[4], Ch. Rajyalakshmi[5] and V. Jayalakshmi[6,*]

[1]Department of Physics, Prasad V. Potluri Siddhartha Institute of Technology, Vijayawada-520007, India
[2]Department of Physics, P.B. Siddhartha Arts & Science College, Vijayawada-520010, India
[3]Department of BS & H, Seshadri Rao Gudlavalleru Engineering College, Gudlavalleru-521356, India
[4]Department of Physics, Lakireddy Bali Reddy College of Engineering, Mylavaram, India
[5]Department of Basic Sciences, Vishnu Institute of Technology, Bhimavaram, India
[6]Department of Physics, National Institute of Technology, Warangal-506004, India

*Corresponding author: E-mail: vlakshmij@gmail.com

Received: 11 May 2023; *Accepted*: 12 June 2023; *Published online*: 31 July 2023; AJC-21314

The hydrothermal approach was used to make an inorganic semiconducting CdS/$Zn_3(PO_4)_2$ nanocomposite at a mild reaction temperature of 100 ºC. The XRD data indicate peaks that correspond to CdS hexagonal structure and $Zn_3(PO_4)_2$ monoclinic-phase with good crystalline character. Surprisingly, the phase shift from α-phase of $Zn_3(PO_4)_2$ to γ-phase of $Zn_3(PO_4)_2$ is observed under hydrothermal conditions due to the coupling of CdS with $Zn_3(PO_4)_2$, as well as internal structural alterations leading to the formation of CdS/$Zn_3(PO_4)_2$ nanocomposite. Debye-Scherrer and W-H methods were used to calculate average crystallite size, lattice strain and dislocation density. The average crystal lattice is 15-25 nm in size. The hexagonal spheres aggregated on rectangular flakes, indicating core-shell heterostructure, may be seen on the surface morphology of the prepared composite. Due to the quantum size effect, the absorption peak for the composite is in the visible wavelength. It also has a low optical band gap of 2.42 eV, which makes it useful for photocatalytic and photoelectrochemical applications. FT-IR spectrum shows all the fundamental vibrational modes of CdS/$Zn_3(PO_4)_2$ nanocomposite. Colour coordinate values and CCT values of the prepared composites indicate that they are used for LED applications and the photoluminescence spectrum reveals a broad, intense luminescence band in the visible region with wavelengths ranging from 510 to 518 nm, in good agreement with the absorption wavelength and the CIE diagram.

Keywords: Hydrothermal synthesis, Cadmium sulphide, Zinc phosphate, Luminescence, Nanocomposite.

INTRODUCTION

A wide range of technologies, including photovoltaic cells, LEDs, sensors, phototransistors, lasers, memory devices, switches, electronics, and the biomedical field, can make use of nanoparticles because of their size-dependent properties [1,2]. Nanocrystalline materials are fascinating because they differ from their bulk counterparts in terms of strength, chemical activity, physical, spectral, optical, magnetic and mechanical properties. In comparison to their bulk counterparts, atoms have a high surface occupancy and their structural features and energy bandgap, semiconducting materials great interest in basic fundamental research and industrial development. The study of nanostructured materials is a significant source for developing new ideas, techniques and methodologies, potentially leading to break-through in major scientific challenges for the development of smart electronic devices [3-5].

Cadmium sulphide (CdS) has a distinct band structure among inorganic semiconductors and has a 2.42 eV indirect energy bandgap (II-VI group) semiconductor with an excited Bohr radius of 5.8 nm. Due to its excellent visible light absorption property, CdS nanoparticles have potential applications in a variety of fields, including light emitting diodes, lasers, photonics, photo catalysis, window layers in solar cells, photovoltaic cells, memory devices, switching devices, hydrogen storage, water and air purification [6,7]. Zinc phosphate is a multifunctional, non-

toxic, anti-corrosion and eco-friendly material. Because of its broad optical band and monoclinic crystal structure, $Zn_3(PO_4)_2$ is an excellent host material for luminescence applications such as optical communication, luminous display systems and as a corrosion resistance material [8-10].

In reality, as compared to separate material systems, composite materials are a better choice for engineering materials and have better qualities. As a result, nanocomposites based on $Zn_3(PO_4)_2$ and CdS have been discovered to be promising materials for novel products in a variety of applications. Novel $CdSZn_3(PO_4)_2$ nanocomposites are being developed in order to improve their functional features. Zinc phosphate decreases the toxicity of CdS and increases the corrosion resistance of $CdSZn_3(PO_4)_2$nanocomposite. The sol-gel, electrochemical, chemical precipitation, sputtering, pulsed laser deposition, metal-organic, chemical vapour deposition, spray pyrolysis, spin coating, dip coating and hydrothermal methods are few techniques that can be used to make these nanophosphate composites.

The hydrothermal treatment is a straightforward approach for producing nanoparticles from aqueous solutions at high pressures and temperatures [11-13]. Using this method, we can decrease particle agglomeration and produce narrow-size, uniformly distributed and mono-dispersed particles with regulated size, shape and dispersibility, which are necessary for further functionalization of the nanomaterials. In this work, a hydrothermal method is applied to prepare CdS, $Zn_3(PO_4)_2$ and CdS-$Zn_3(PO_4)_2$ nanocomposite. The hexagonal phase in pure CdS and the monoclinic phase in $Zn_3(PO_4)_2$ are confirmed by X-ray and the $CdSZn_3(PO_4)_2$ nanocomposite reveals both hexagonal and monoclinic phases with a minor change in the lattice parameters. Debye-Scherrer equation and W-H plot are used to compute average crystallite size, microstrain and dislocation densities. The existence of functional groups and their positions are revealed by FTIR. The SEM reveals hexagonal spheres in CdS, rectangular flakes in $Zn_3(PO_4)_2$ and spherical morphologies in $CdSZn_3(PO_4)_2$. The presence of component constituents of the substance is confirmed by EDAX analysis. The coupling effect and local structural alterations are evident in the UV-Vis diffused reflectance measurements. At a wavelength of 518 nm, photoluminescence emits strongly. The produced nanocomposites may be employed for white light emitting diodes, according to the CIE colour coordinates (WLEDs).

EXPERIMENTAL

To prepare $CdSZn_3(PO_4)_2$ nanocomposite, all the chemicals and reagents were of analytical grade and have a purity of > 99%. Precursor materials for synthesis include cadmium nitrate tetrahydrate ($Cd(NO_3)_2{\cdot}4H_2O$), thiourea (CH_4N_2S) and zinc phosphate ($Zn_3(PO_4)_2$).

Synthesis: In this method, $Cd(NO_3)_2{\cdot}4H_2O$, thiourea and $Zn_3(PO_4)_2$ were dissolved in a solution containing 40 mL of distilled water and 20 mL of ethanol with constant stirring at room temperature. After 10 min, added NaOH solution drop by drop to the aforementioned solution and stirred constantly further for 2 h to achieve uniformity without aggolemarization. A white solution has become light yellow suggested the formation of CdS/$Zn_3(PO_4)_2$ nanocomposite. This solution was put into 150 mL stainless steel Teflon walled autoclaves and autogenously pressured for 3 h in a hot air oven at 100 ºC. It was allowed to cool to room temperature before being washed multiple times with distilled water, filtered and dried in a hot air oven for 6 h at 60 ºC. Finally, the prepared samples were grinded to get a smooth powder.

Characterization: Powder X-ray diffraction (PXRD) patterns were recorded in the scanning range of 20-90º (2θ), using Cu*K*α radiation with a wavelength of 1.5406 Å, using PAN analytical, X' Pert PRO model at room temperature and structural analysis, crystal lattice size and phase identification of synthesized samples were analyzed using X' Pert Pro software. Using a Fourier Transform infrared spectrophotometer (SHIMADZU-IR, Affinity-1S FT-IR spectrophotometer) in the middle infrared range 4000-400 cm^{-1} at room temperature, various functional groups and molecular vibrations contained in the prepared samples were carefully studied. The morphological and chemical composition of CdS, $Zn_3(PO_4)_2$, $CdSZn_3(PO_4)_2$ nanopowders were determined using a scanning electron microscope (SEM; TESCAN, VEGA3 LMU model) with an accelerating voltage of 15 kV and EDAX acquisition. To determine the optical band gap of current samples, diffused reflectance spectra (DRS) in the wavelength range of 300-1000 nm were obtained using a UV-Vis spectrophotometer (SPECORD–210 plus, Analytic Jena) and the spectra were converted from the reflection function to the absorbance function using the Kubelka-Munk method. The photoluminescence spectra in a PERKIN ELMER LS-55 with a Xenon lamp of excitation 325 nm were obtained to investigate the emission properties. Furthermore, colour chromaticity experiments were carried out in order to determine the relevance of colour coordinates and colour correlated temperature (CCT) for future optoelectronic device applications.

RESULTS AND DISCUSSION

Structural and morphological properties

X-ray diffraction: Fig. 1 shows the XRD patterns of CdS, $Zn_3(PO_4)_2$ and CdS/$Zn_3(PO_4)_2$ nanocomposite. The strong and narrow peaks indicate high crystallinity of the prepared materials. CdS has a hexagonal phase, pure $Zn_3(PO_4)_2$ has a monoclinic γ-phase and CdS/$Zn_3(PO_4)_2$ composite contains both hexagonal and intermixing γ,β-monoclinic phases coexist. In CdS/$Zn_3(PO_4)_2$ nanocomposite, X-ray peaks are observed inter-mixing state of both γ,β-phase of monoclinic zinc phosphate matched with the standard powder XRD data of γ-phase (JCPDS #30-1490) and β-phase (JCPDS #30-1489). Some of the peaks in the XRD pattern matched with the hexagonal structure of CdS standard XRD data (JC-PDS file No: 65-3414). There is a phase change of zinc phosphate from γ-phase to γ and β inter-mixing phase due to the interaction of CdS and $Zn_3(PO_4)_2$ under hydrothermal synthesis conditions, without affecting the hexagonal phase of CdS [14,15].

When comparing pure CdS and $Zn_3(PO_4)_2$ samples, there is an appropriate change in peak position in CdS/$Zn_3(PO_4)_2$ composite samples. This clearly shows that CdS molecules

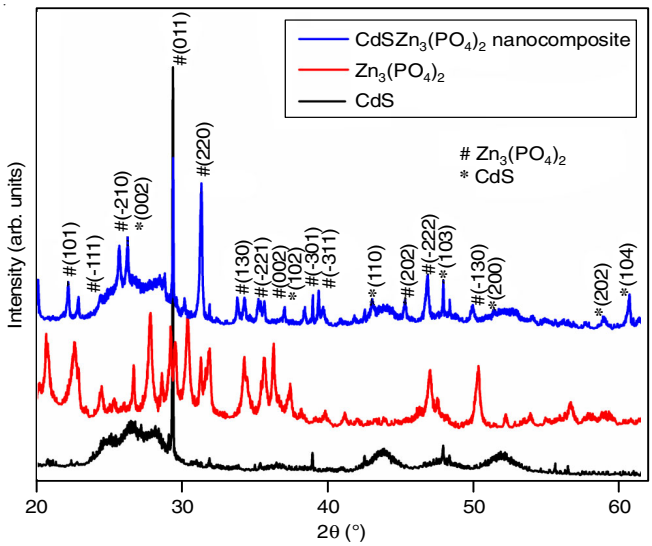

Fig. 1. Powder X-ray diffraction pattern of pure CdS, pure $Zn_3(PO_4)_2$ and CdS/$Zn_3(PO_4)_2$ nanocomposite

combined with $Zn_3(PO_4)_2$ produce CdS/$Zn_3(PO_4)_2$ nanocomposite, results in the changes of peak locations of stress, whether tensile or compressive, have far-reaching effects on the nanocomposite's local disorder and microstructure. This can be understood from the atomic radius of CdS is ~ 0.97 Å and $Zn_3(PO_4)_2$ ~ 0.74 Å, they may occupy the regular lattice site of pure CdS and $Zn_3(PO_4)_2$ react as CdS-$Zn_3(PO_4)_2$ composite. A broad nature of intense peaks strongly suggests that the crystallite sizes of samples are nanoscale. While the modest shift in peak locations indicates the presence of local disorder and lattice strain in nanocomposites [16,17], there is also a change in lattice parameters and phase distribution (Table-1). Debye-Scherrer's formula was used to calculate the average size of a crystal lattice by considering the full width at half-maximum of the diffraction peaks:

$$D = \frac{k\lambda}{\beta\cos\theta}$$

where k is shape factor; D is the average size of crystal lattice; λ is the wavelength of X-rays; β is the full-width of half maximum (FWHM) of X-ray diffraction peaks and θ is the Bragg's diffraction angle.

The induced strain (ε) is calculated using Stokes-Wilson equation [18]:

$$\varepsilon = \frac{\beta}{4\tan\theta}$$

Stress (ε) is not taken into account in Debye-Scherrer's equation for calculating crystallite size, therefore particles are assumed to be stress-free. To estimate average crystal lattice size and microstrain, the Williamson and Hall (W-H) approach is used, which involves de-convolution of both induced size and strain broadening by measuring the width of the peak as a function of 2θ [19].

The Williamson and Hall (W-H) equation is expressed as:

$$\beta\cos\theta = \frac{0.9\lambda}{D} + 4\varepsilon\sin\theta$$

In Fig. 2, 4sin θ *versus* βcos θ for CdS, $Zn_3(PO_4)_2$ and CdS/$Zn_3(PO_4)_2$ nanocomposite are shown. Microstrain and crystallite sizes were calculated from the slope and intercept, respectively, using a straight line fit of the data. The dislocation density (δ) was calculated using the following formula:

$$\delta = \frac{1}{D^2}$$

TABLE-1
PHASE, LATTICE PARAMETERS, VOLUME OF UNIT CELL AND AXES OF SYMMETRY OF X-RAY DIFFRACTION PATTERNS OF PURE CdS, $Zn_3(PO_4)_2$, CdS/$Zn_3(PO_4)_2$ NANOCOMPOSITES UNDER HYDROTHERMAL METHOD

Sample code	Phase	CdS				
		Lattice parameters (Å)			Volume of unit cell	Axes of symmetry
		a	b	c	$(3a^2c/2)$ Sin γ (abc)	α = β = 90° and γ
CdS	Hexagonal	4.128	4.128	6.78	173.3	119.97°
$Zn_3(PO_4)_2$	Monoclinic γ-phase	7.423	8.149	5.12	342.0	119.85°
$CdSZn_3(PO_4)_2$ composite	Hexagonal and Monoclinic γ, β phase	4.123	4.123	6.82	174.0	119.97°
		7.549	8.499	5.04	320.0	108.03°
JCPDS (65-3414)		4.132	4.132	6.73	172.3	120.00°
JCPDS (30-1489)		7.549	8.499	5.04	607.0	112.80°
JCPDS (30-1490)		9.175	8.260	8.86	322.0	95.03°

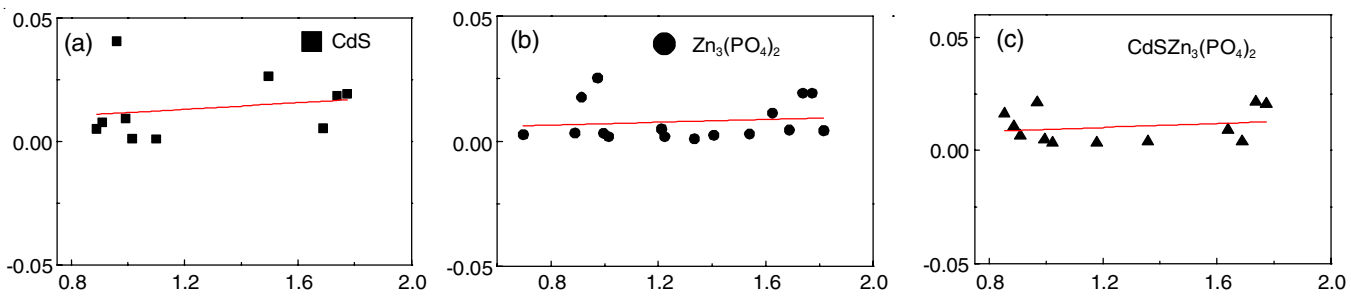

Fig. 2. W-H plot of CdS, $Zn_3(PO_4)_2$ and CdS/$Zn_3(PO_4)_2$ nanocomposite

TABLE-2
AVERAGE CRYSTALLITE SIZE, LATTICE STRAIN AND DISLOCATION DENSITY OF PURE CdS, PURE $Zn_3(PO_4)_2$ AND CdS/$Zn_3(PO_4)_2$ FROM DEBYE-SCHERRER AND W-H PLOT CALCULATIONS

Sample code	Crystallite size (nm)		Lattice strain ($\varepsilon \times 10^{-4}$)		Dislocation density ($\delta \times 10^{15}$ m^{-2})	
	Scherrers	W-H plot	Scherrers	W-H plot	Scherrers	W-H plot
CdS	17.44	18.92	10.08	12.41	3.28	2.79
$Zn_3(PO_4)_2$	13.54	15.36	13.05	14.32	5.45	4.25
$CdSZn_3(PO_4)_2$	22.96	24.52	9.25	13.44	1.89	1.43

The crystallite size, microstrain and dislocation density as determined by Debye-Scherrer's and W-H plots are presented in Table-2.

FTIR studies: Fig. 3 shows the FTIR spectrum used to evaluate the existence of distinct vibrational modes in CdS, $Zn_3(PO_4)_2$ and CdS/$Zn_3(PO_4)_2$ nanopowders. Table-3 shows the various peak positions attributed to their associated functional groups and basic vibrational modes. A large drop occurs at 3368 cm^{-1} owing to O-H Stretching due to the strong interaction of water with the CdS lattice surface and a sharp peak appears at 1633 cm^{-1} owing to the adsorbed water H-O-H bending mode [20]. A peak at 1025 cm^{-1} indicates sulfate formation.

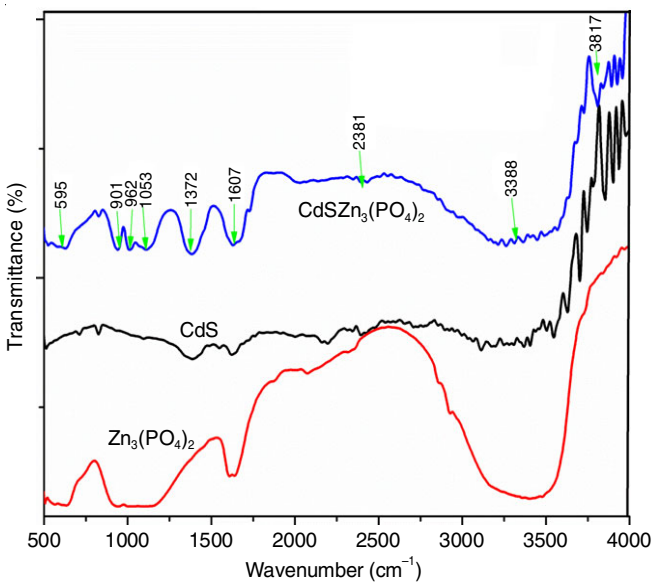

Fig. 3. FT-IR spectra for pure CdS, pure $Zn_3(PO_4)_2$, $CdSZn_3(PO_4)_2$ nanocomposites

The existence of water is established by its 1608 cm^{-1} bending vibration. At 848 cm^{-1}, there is a weak peak caused by C-H stretching. A complex of stretching of PO_4^{3-} group is reported by the existence of multiple strong and sharp absorption bands from 800 to 1200 cm^{-1} that break into three peaks. The anti-symmetric stretching and symmetric stretching of PO_4^{3-} were due to the absorption bands at 1040 and 1112 cm^{-1}, respectively. The anti-symmetric stretching of PO_4^{3-} and P-O bending appeared at broad peaks at 586 and 592 cm^{-1}, respectively [21]. The most distinctive signature peak is appeared at 2381 cm^{-1}, which results due to the addition of water to CdS sample. An S-H vibration peak is observed when CdS nanoparticles become stabilized by water, providing a conclusive proof of this interaction.

TABLE-3
INFRARED VIBRATIONAL ASSIGNMENT OF PEAK POSITIONS, INTENSITY WITH ITS CORRESPONDING FREQUENCY REGION FOR PURE CdS, PURE $Zn_3(PO_4)_2$ AND CdS/$Zn_3(PO_4)_2$ NANOCOMPOSITES

Vibrational frequency (cm^{-1})			Band assignment
CdS	$Zn_3(PO_4)_2$	$CdSZn_3(PO_4)_2$	
–	586	592	P-O Symmetric stretching mode
848	850	901	C-H Stretching
972	945	962	Asymmetric P-O stretching mode
1025	1021	1053	C-O, S-O anti-symmetric
-	1040	1112	Symmetric stretching of PO_4^{3-}
1370	1294	1372	CH_3
1608	1547	1607	O-H bending vibration
1776	1782	1775	O-H bending vibration
2384	2341	2381	S-H BOND
3368	3345	3388	Intermolecular bonds
3827	3798	3817	Vibrations of O-H stretching absorbed water on the surface of the samples

Morphological studies: SEM images of CdS, $Zn_3(PO_4)_2$ and CdS/$Zn_3(PO_4)_2$ nanocomposites are shown in Fig. 4, where pure CdS morphology shows hexagonal spheres with aggregation, whereas pure $Zn_3(PO_4)_2$ morphology shows tiny rectangular flakes like structure. The morphology of CdS/$Zn_3(PO_4)_2$ nanocomposite is heterostructure, as CdS nanoparticles are distributed discretely and evenly in the shape of hexagonal spheres over the surfaces of rectangular $Zn_3(PO_4)_2$ flakes. Moreover, due to the coupling of optically active CdS material with $Zn_3(PO_4)_2$, the size of the flakes in this nanocomposite is enhanced as compared to pure flakes. This type of nanoscale heterostructure morphology could lead to the discovery of new physical effects, as well as cardinal improved characteristics for commonly used semiconductor devices such as photo diodes, solar cells, lasers and LEDs, as well as the development of new, more efficient devices [22,23].

Fig. 5 shows the elemental chemical composition of CdS, $Zn_3(PO_4)_2$ and $CdSZn_3(PO_4)_2$ nanocomposite samples evaluated by EDAX. There are no additional trace elements other than the fundamental components, as seen by the distinct peaks of cadmium, sulphate and zinc phosphate (Zn, P and O). The stoichiometry ratio of the reactant combination as almost equivalent to the composition ratio of CdS:$Zn_3(PO_4)_2$.

Optical properties

Diffusion reflectance spectra: The reflection spectra acquired in the wavelength range 200-800 nm were used to estimate the bandgap measurements. The estimated bandgap for $Zn_3(PO_4)_2$, CdS and $CdSZn_3(PO_4)_2$ obtained from a plot of

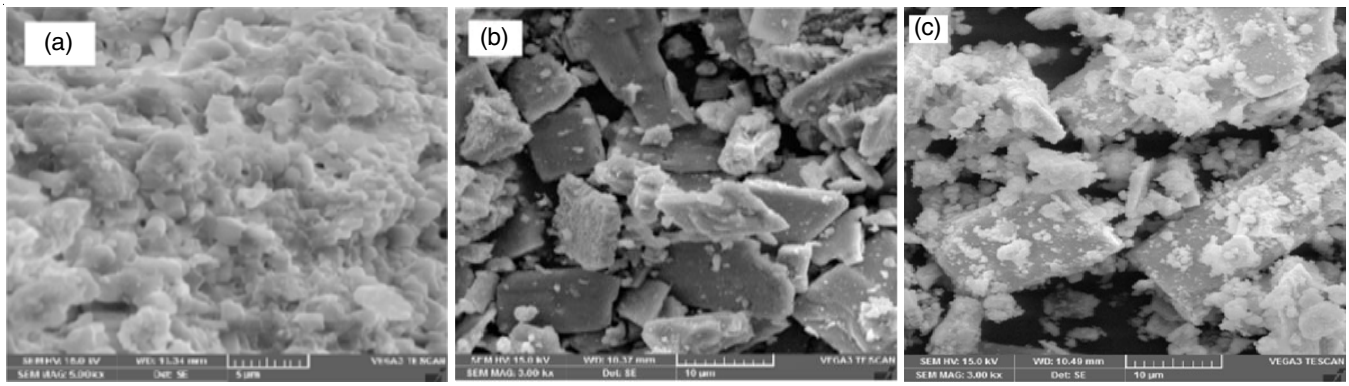

Fig. 4. SEM micrographs for (a) CdS, (b) $Zn_3(PO_4)_2$, (c) $CdS/Zn_3(PO_4)_2$ nanocomposite

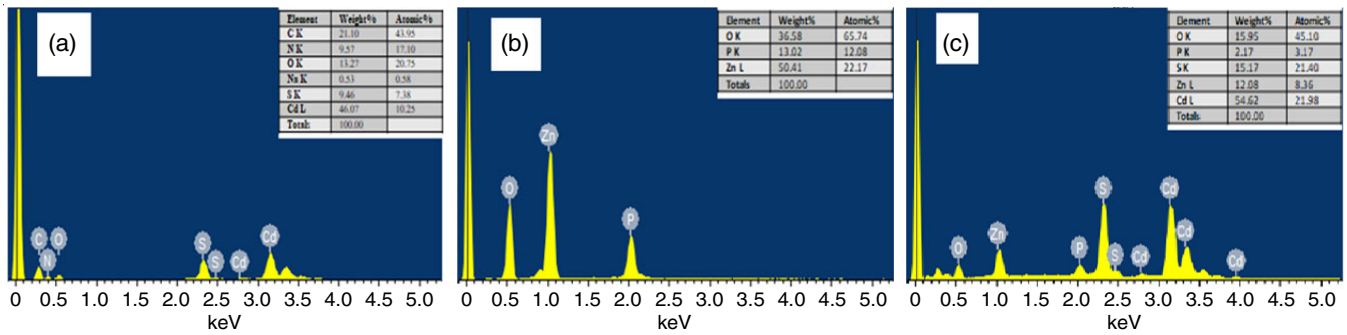

Fig. 5. EDAX Images for (a) pure CdS, (b) pure $Zn_3(PO_4)_2$, (c) $CdSZn_3(PO_4)_2$ nanocomposites

F(R) against hν at room temperature is shown in Fig. 6. The Kubelka-Munk model [24] was used to calculate the bandgap of CdS, $Zn_3(PO_4)_2$ and $CdSZn_3(PO_4)_2$ nanoparticles and is represented as:

$$F(R) = \frac{(1-R)^2}{2R}$$

where R is absolute reflectance of the sample.

The energy band gap of pure CdS, pure $Zn_3(PO_4)_2$ and $CdSZn_3(PO_4)_2$ nanocomposite, with a bandgap of 2.25 eV, CdS has a strong reflection band in the visible range. With a bandgap of 2.48 eV and a minor blue shift, $CdS/Zn_3(PO_4)_2$ nanocomposite reacted effectively to visible light as well. Since the Fermi-level in semiconductors lies between two bands, low-energy optical and electrical behaviour is dominated by the edges of the bands. Even for crystallites with 10,000 atoms, the optical excitations across the gap are highly dependent on their size. The band gap of semiconductor nanoparticles, which narrows with increasing size and causes the interband transition to occur at higher frequencies, is particularly susceptible to the quantum size effect [25]. It is a handy approach for identifying semiconductor nanoparticles that have a quantum size effect induced by photo-generated electron-hole pairs. The UV-visible reflection spectrum of semiconductor nanoparticles is size dep-

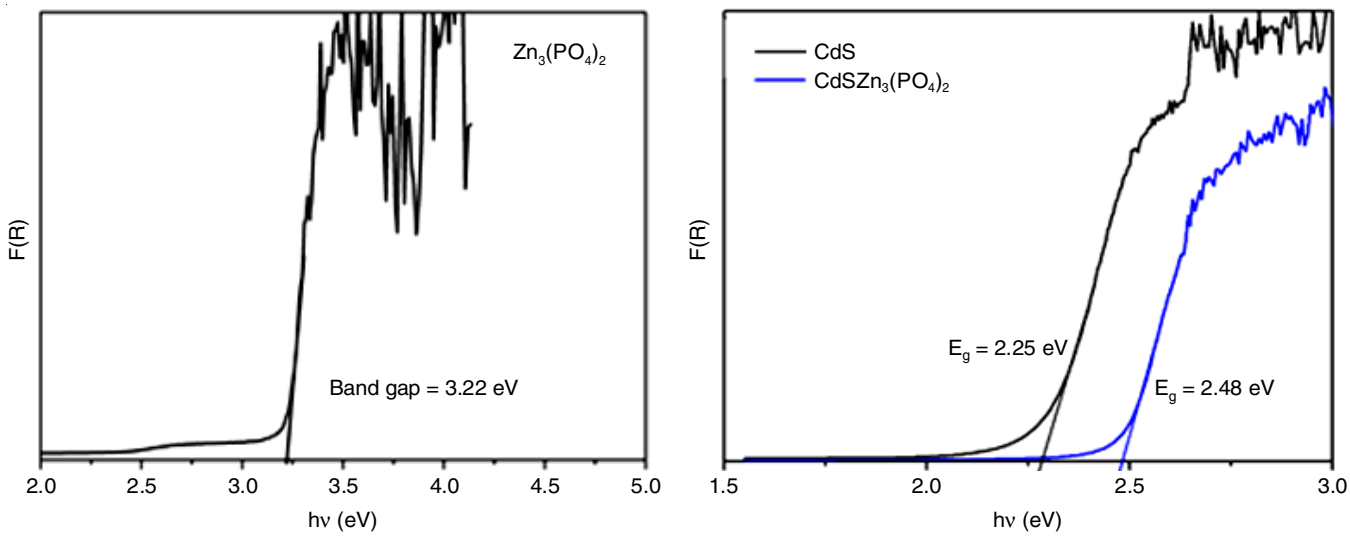

Fig. 6. UV-Vis diffuse reflectance spectra of CdS, $Zn_3(PO_4)_2$ and $CdSZn_3(PO_4)_2$ nanocomposite

endent and the reflection maximum diminishes as nanoparticle size increases [26,27].

Photoluminescence studies: Fig. 7 shows the photoluminescence (PL) spectrum of CdS, CdS/$Zn_3(PO_4)_2$. According to photoluminescence theory, excitonic emission is acute at the absorption edge, whereas trapped emission is wide at longer wavelengths. CdS has a broad peak at 528 nm, whereas CdS/$Zn_3(PO_4)_2$ nanocomposite has a broad band at 518 nm, which is attributable to trapped luminescence or near band edge (NBE) emission. The emission associated with the electronic transition from the conduction band to an accepter level created by interstitial sulphur ions has a green emission band at 518 nm [28, 29]. Excitation from S interstitial [Is] to the conduction band causes the peak at 518 nm to be referred to as green emission. Sulphur's *s*- and *p*-orbitals dominate the valence band in CdS, whereas cadmium's *s*-orbitals dominate the conduction band [30]. InCdS, sulphur vacancies (Vs) are localized sites immediately below the conduction band (CB), whereas the interstitial sulphur (Is) is found above the valence band (VB). The high crystallinity of the prepared CdS/$Zn_3(PO_4)_2$ nanocomposites is supported by the XRD diffraction pattern and PL spectra. As a result, the hexagonal CdS/$Zn_3(PO_4)_2$ photocatalyst should have a high photocatalytic degradation efficiency.

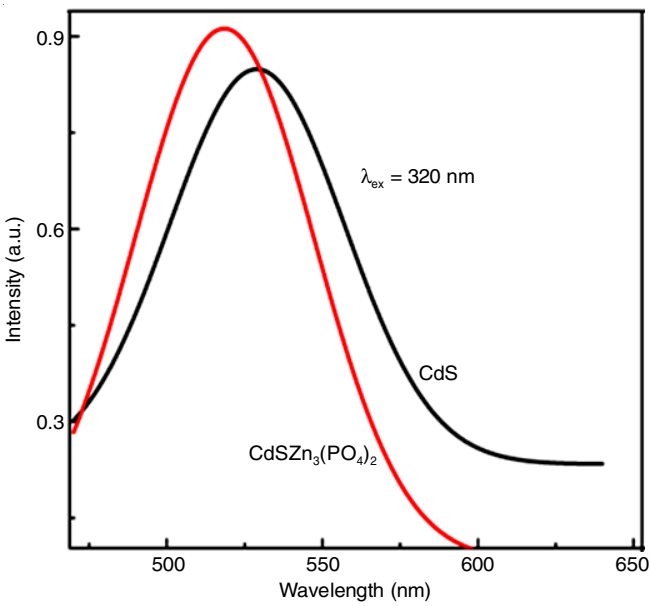

Fig. 7. Photoluminescence spectrum of CdS and $CdSZn_3(PO_4)_2$ nanocomposite

To investigate the colour emission of CdS and $CdSZn_3(PO_4)_2$, CIE (Commission Internationale de L'Eclariage) chromacity coordinates were calculated and the colour of these materials is depicted in Fig. 8. Colour chromaticity coordinates for CdS, $CdSZn_3(PO_4)_2$ nanocomposite are $x = 0.1221$, $y = 0.7866$; and $x = 0.0899$, $y = 0.7724$, respectively. CIE coordinates show the green emission indicated as A, B. The CCT (colour correlated temperature) values were calculated using the McCamy empirical method [31] to investigate the quality of light emission.

$$CCT = -437n^3 + 3601n^2 - 6861n + 5514{:}31$$

where $n = (x - x_e)/(y - y_e)$ and the chromaticity epicentre is at $x_e = 0.3320$ and $y_e = 0.1858$ and (x,y) are the nanocomposite

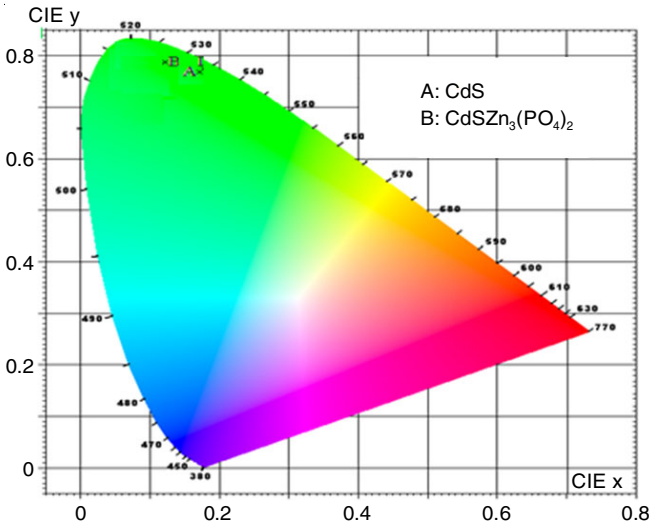

Fig. 8. CIE diagram of CdS, $CdSZn_3(PO_4)_2$ nanocomposite

colour coordinates. Table-4 shows the colour coordinates, CCT values and corresponding wavelengths. In general, the cool white light emission employed in commercial LED applications is indicated by (CCT value > 5000 K) [32].

TABLE-4
CALCULATED WAVELENGTH, COLOUR COORDINATES, CCT VALUES FROM PL SPECTRA OF PURE CdS, $Zn_3(PO_4)_2$ AND CdS/$Zn_3(PO_4)_2$ NANOCOMPOSITES

Sample code	Wavelength (nm)	Colour coordinates		CCT (K)
		x	y	
CdS	523	0.1221	0.7866	8260
$CdSZn_3(PO_4)_2$	518	0.0899	0.7724	8879

Conclusion

In summary, the hydrothermal method was employed to synthesize CdS/$Zn_3(PO_4)_2$ nanocomposite using CdS and $Zn_3(PO_4)_2$. XRD confirms hexagonal phase in CdS and monoclinic phase in $Zn_3(PO_4)_2$ while $CdSZn_3(PO_4)_2$ nanocomposite shows both hexagonal and monoclinic phase with a slight variation in the lattice parameters of nanocomposite. Debye-Scherrer equation and W-H plot were used to compute average crystallite size, microstrain and dislocation densities. The existence of fundamental modes of functional groups may be seen in FT-IR spectra. SEM images at various magnifications revealed hexagonal spheres in CdS, rectangular flakes in $Zn_3(PO_4)_2$ and spherical morphologies in CdS/$Zn_3(PO_4)_2$. The EDAX analysis confirms the presence of constituent elements of the material. The coupling effect and local structural alterations are readily seen in the UV-Vis diffused reflectance measurements. At an excitation wavelength of 325 nm, photoluminescence spectra show a broad strong emission wavelength of 518 nm. The produced nanocomposites may be employed for white light emitting diodes, according to the CIE colour coordinates (WLEDs).

CONFLICT OF INTEREST

The authors declare that there is no conflict of interests regarding the publication of this article.

REFERENCES

1. M. Lee, H. Seung, J.I. Kwon, M.K. Choi, D.-H. Kim and C. Choi, *ACS Omega*, **8**, 5209 (2023); https://doi.org/10.1021/acsomega.3c00440
2. P. Kumbhakar, C.C. Gowda and C.S. Tiwary, *Front. Mater*., **8**, 721514 (2021); https://doi.org/10.3389/fmats.2021.721514
3. T. Maldiney, A. Bessière, J. Seguin, E. Teston, S.K. Sharma, B. Viana, A.J. Bos, P. Dorenbos, M. Bessodes, D.J.N. Gourier, D. Scherman and C. Richard, *Nat. Mater.*, **13**, 418 (2014); https://doi.org/10.1038/nmat3908
4. Y.-C. Liang and T.-W.J.N.R.L. Lung, *Nanoscale Res. Lett.*, **11**, 264 (2016); https://doi.org/10.1186/s11671-016-1490-x
5. D. Ayodhya and G.J.J.S.A.M. Veerabhadram, *J. Sci. Adv. Mater. Devices*, **4**, 381 (2019); https://doi.org/10.1016/j.jsamd.2019.08.006
6. G.J.J. Murugadoss, *J. Lumin.*, **146**, 430 (2014); https://doi.org/10.1016/j.jlumin.2013.09.052
7. C. Tiwary, R. Sarkar, P. Kumbhakar and A.J.P.L.A. Mitra, *Phys. Lett. A*, **372**, 5825 (2008); https://doi.org/10.1016/j.physleta.2008.07.036
8. B. Yan and X.J.J.N.R. Xiao, *J. Nanopart. Res.*, **11**, 2125 (2009); https://doi.org/10.1007/s11051-008-9578-6
9. M. Elias, S. Akter, M.A. Hossain and M.H.J.T.S.F. Suhag, *Thin Solid Films*, **717**, 138472 (2021); https://doi.org/10.1016/j.tsf.2020.138472
10. B. del Amo, R. Romagnoli, V. Vetere and L.J.P.O.C. Hernández, *Prog. Org. Coat.*, **33**, 28 (1998); https://doi.org/10.1016/S0300-9440(97)00124-0
11. J. Madhavi, *SN Appl. Sci.*, **1**, 1509 (2019); https://doi.org/10.1007/s42452-019-1291-9
12. J.-J. Dong, C.-Y. Zhen, H.-Y. Hao, J. Xing, Z.-L. Zhang, Z.-Y. Zheng and X.-W.J.N. Zhang, *Nanoscale Res. Lett.*, **8**, 378 (2013); https://doi.org/10.1186/1556-276X-8-378
13. B. Rajesh Kumar and B. Hymavathi, *J. Asian Ceram. Soc.*, **5**, 94 (2017); https://doi.org/10.1016/j.jascer.2017.02.001
14. N. Zhang, X. Ma, Y. Yin, Y. Chen, C. Li, J. Yin and S. Ruan, *Inorg. Chem. Front.*, **6**, 238 (2019); https://doi.org/10.1039/C8QI00951A
15. B. Zhu, F. Wang, Y. Cao, C. Wang, J. Wang and Y. Gu, *Appl. Phys. Lett.*, **108**, 252106 (2016); https://doi.org/10.1063/1.4954716
16. T. Xie, H. Guo, J. Zhang, Y. He, H. Lin, G. Chen and Z.J.J.L. Zheng, *J. Lumin.*, **170**, 150 (2016); https://doi.org/10.1016/j.jlumin.2015.10.044
17. W. Zhao, C. Tian, Z. Xie, C. Wang, W. Fu and H.J.F.M.S. Yang, *Front. Mater. Sci.*, **11**, 271 (2017); https://doi.org/10.1007/s11706-017-0393-9
18. R. Joyce Stella, G. Thirumala Rao, V. Pushpa Manjari, B. Babu, C. Rama Krishna and R.V.S.S.N. Ravikumar, *J. Alloys Compd.*, **628**, 39 (2015); https://doi.org/10.1016/j.jallcom.2014.11.201
19. S.K. Muswareen, M.S. Rao, G. Sridevi and S.J.M.S.S.P. Cole, *Mater. Sci. Semicond. Process.*, **102**, 104588 (2019); https://doi.org/10.1016/j.mssp.2019.104588
20. B. Minèeva-Šukarova, B. Mangovska, G. Bogoeva-Gaceva and V.M.J.C.C.A. Petruševski, *Croat. Chem. Acta*, **85**, 63 (2012); https://doi.org/10.5562/cca1888
21. S. Yuvaraj, A.C. Fernandez, M. Sundararajan, C.S. Dash and P.J.C.I. Sakthivel, *Ceram. Int.*, **46**, 391 (2020); https://doi.org/10.1016/j.ceramint.2019.08.274
22. S. Ouendadji, S. Ghemid, H. Meradji and F.E.H. Hassan, *Comput. Mater. Sci.*, **50**, 1460 (2011); https://doi.org/10.1016/j.commatsci.2010.11.035
23. A.M.A. Al-Hussam and S.A.-J. Jassim, *J. Assoc. Arab Univ. Basic Appl. Sci.*, **11**, 27 (2012); https://doi.org/10.1016/j.jaubas.2011.10.001
24. H. Jamil, I. Dildar, U. Ilyas, J. Hashmi, S. Shaukat, M. Sarwar and M. Khaleeq-ur-Rahman, *Thin Solid Films*, **732**, 138796 (2021); https://doi.org/10.1016/j.tsf.2021.138796
25. A.A. Christy, O.M. Kvalheim and R.A.J.V.S. Velapoldi, *Vib. Spectrosc.*, **9**, 19 (1995); https://doi.org/10.1016/0924-2031(94)00065-O
26. G.T. Rao, B. Babu, R.J. Stella, V.P. Manjari, C.V. Reddy, J. Shim and R.V.S.S.N. Ravikumar, *J. Mol. Struct.*, **1081**, 254 (2015); https://doi.org/10.1016/j.molstruc.2014.10.044
27. A. Ganguly and S.J.M.S. Nath, *Mater. Sci. Eng. B*, **255**, 114532 (2020); https://doi.org/10.1016/j.mseb.2020.114532
28. W. Chen, Y. Sun, J. Ge, F. Song, Y. Xie, Y. Zheng and P. Rao, *Cryst. Eng. Commun.*, **23**, 8291 (2021); https://doi.org/10.1039/D1CE01007G
29. G. Sreedevi, K. Srinivas, M. Subbarao and S. Cole, *J. Mol. Struct.*, **1222**, 128903 (2020); https://doi.org/10.1016/j.molstruc.2020.128903
30. K. Raviteja, N. Sreelekha, D.A. Reddy, R. Vijayalakshmi and K.J.A.S.L. Subramanyam, *Adv. Sci. Lett.*, **24**, 5657 (2018); https://doi.org/10.1166/asl.2018.12170
31. C.S.J.C.R. McCamy, *Color Res. Appl.*, **17**, 142 (1992); https://doi.org/10.1002/col.5080170211
32. P.O. Anikeeva, J.E. Halpert, M.G. Bawendi and V. Buloviæ, *Nano Lett.*, **9**, 2532 (2009); https://doi.org/10.1021/nl9002969